Electronic Transport and Quantum Hall Effect in Bipolar Graphene *p-n-p* Junctions

Barbaros Özyilmaz,[1,*] Pablo Jarillo-Herrero,[1,*] Dmitri Efetov,[1] Dmitry A. Abanin,[2] Leonid S. Levitov,[2] and Philip Kim[1,†]

[1]*Department of Physics, Columbia University, New York, New York 10027, USA*

[2]*Department of Physics, Center for Materials Sciences and Engineering, Massachusetts Institute of Technology, Cambridge, Massachusetts 02139, USA*

(Received 8 August 2007; published 17 October 2007)

We have developed a device fabrication process to pattern graphene into nanostructures of arbitrary shape and control their electronic properties using local electrostatic gates. Electronic transport measurements have been used to characterize locally gated bipolar graphene *p-n-p* junctions. We observe a series of fractional quantum Hall conductance plateaus at high magnetic fields as the local charge density is varied in the *p* and *n* regions. These fractional plateaus, originating from chiral edge states equilibration at the *p-n* interfaces, exhibit sensitivity to interedge backscattering which is found to be strong for some of the plateaus and much weaker for other plateaus. We use this effect to explore the role of backscattering and estimate disorder strength in our graphene devices.

DOI: 10.1103/PhysRevLett.99.166804 PACS numbers: 81.05.Uw, 73.63.−b

Graphene, a recently discovered single sheet of graphite [1], stands out as an exceptional material both in terms of the fundamental physics associated with its unique "quasirelativistic" carrier dynamics and potential applications in electronic devices [2]. Most experiments to date have depended on the presence of a heavily doped Si substrate which serves as a global back gate, inducing charge density via the electric field effect. Although such global gate approach yields interesting transport phenomena [1,3–7], it represents only the first step toward more complex graphene devices. The use of local gates enables the fabrication of in-plane graphene heterostructures [8,9]. A number of applications for local gate devices have been proposed in order to investigate Klein tunneling [10], electron Veselago-lens [11], quantum point contacts [12], and quantum dots [13,14].

In this Letter, we study locally gated graphene devices in the quantum Hall (QH) regime. By independently varying voltage on the back gate and local gate, we can study bipolar QH transport in graphene *p-n-p* heterojunctions in different charge density regimes. We find a series of fractional QH conductance plateaus as the local charge density is varied in the *p* and *n* regions. Recently a similar QH effect has been reported in a single *p-n* graphene heterojunction [15]. Our double junction system allows us to study new interesting transport regimes that are absent in the QH edge transport in a single junction, in particular, partial equilibration of graphene QH edge states. Conspicuously, some of our fractionally quantized plateaus are found to be considerably more fragile with respect to disorder than the other plateaus. We analyze the distinction in the roughness of different plateaus and show that it points to the importance of interedge backscattering in our narrow graphene samples.

Our devices have been fabricated following a combination of an etching and dielectric deposition techniques. Figure 1(a) shows examples of nanostructured graphene devices after the complete fabrication process. The devices consist of a designed graphene nanostructure sandwiched between two dielectrics, with a global back gate (the highly doped Si substrate) and partially covered by one or more local gates [Fig. 1(b)]. Such gates allow us to tune the location of the Fermi energy in graphene globally (via the back gate voltage, V_{BG}) or locally (via the local gate voltage, V_{LG}). The conductance, G, of our devices is measured at cryogenic temperatures (1.5 to 4.2 K), as a function of V_{BG} and V_{LG}, by using a lock-in technique with an ac excitation voltage of 100 μV. The single layer

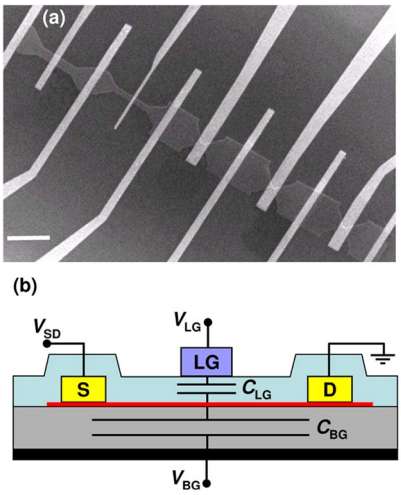

FIG. 1 (color online). (a) Scanning electron microscopy (SEM) picture showing several complete two-probe devices with local gates. Scale bar is 2 μm. The electrodes contact the widest parts of the structure. The local gates cover the graphene constrictions and part of the central graphene bars. (b) Schematic side view of the devices. Graphene is contacted by source (S) and drain (D) electrodes, and separated from the back gate plane by 300 nm SiO_2, and from the local gate (LG) by the top dielectric (20 nm HSQ and 15 nm HfO_2). The back gate (with voltage V_{BG}) is coupled to the entire graphene structure via the capacitor C_{BG}. The local gate only couples to part of the structure via C_{LG}.

character of our devices is determined by Raman spectroscopy [16] and/or quantum Hall effect measurements [3,4].

Bulk graphene is a zero band gap semiconductor. Therefore, the Fermi energy in graphene can be continuously varied from valence to conduction band via the field effect. Incorporating local gates allows us to induce different charge densities at different sample regions. Of particular interest is the case when the Fermi energy in one region is in the valence band (p-type) while in the other region it is in the conduction band (n-type).

We have fabricated graphene p-n-p/n-p-n devices with different gated channel width and length [see Fig. 1(a)]. In total 6 devices in two different single layer graphene pieces were studied and found to exhibit similar characteristics. Figure 2(b) shows $G(V_{\mathrm{LG}}, V_{\mathrm{BG}})$ at zero magnetic field for a typical device [9]. The most prominent feature is the presence of two conductance minima valleys: one approximately horizontal, independent of the voltage V_{LG}, and the other diagonal. The first valley tracks the charge neutrality point (or Dirac point) in the regions outside the local gate, further denoted as graphene leads (GLs). The second valley, whose position is controlled both by the local and the back gate voltage, tracks the neutrality point in the region under the local gate (LGR). The slope of this valley is equal to the ratio of the local capacitance to the back gate capacitance. For the device shown in Fig. 2(b) this ratio is 10.5. Note that the typical local gate breakdown voltage for our dielectric heterostructure is larger than 12 V, which, together with a tenfold enhancement of the gate coupling factor, means that we can induce local charge densities at least comparable, and often larger, than with the back gate (where leakage typically starts to occur at $V_{\mathrm{BG}} \sim 100$ V).

Away from the Dirac valleys, the conductance increases with increasing charge density (see Fig. 2). The two valleys separate four regions in the plot: p-p'-p, p-n'-p, n-n'-n and n-p'-n, where n (p) refers to negative (positive) charge density and the prime indicates density in the LGR. The conductance is not symmetric across the valleys, because

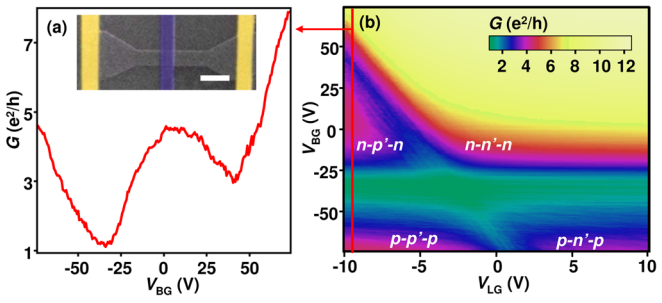

FIG. 2 (color online). (a) $G(V_{\mathrm{BG}})$ for a graphene p-n-p junction, extracted from (b), showing the two conductance minima associated with Dirac valleys in the graphene leads and under the local gate. Inset: false color SEM picture of a patterned graphene bar with contacts and local gate. Scale bar represents 1 μm. (b) Two-dimensional plot of $G(V_{\mathrm{LG}}, V_{\mathrm{BG}})$ for the device shown in (a).

for opposite polarities there is an extra contribution due to the resistance of the two p-n interfaces [9]. We also note here that even in the p-n-p and n-p-n regions, the device shows considerable conductance ($G > e^2/h$) without any signature of rectifying behavior, as expected for transport in a zero-gap heterojunction. In fact, graphene is the only two-dimensional electron gas (2DEG) where in-plane bipolar heterostructures p-n'-p and n-p'-n can be studied in the linear response regime.

The lateral graphene heterojunctions exhibit interesting phenomena at high magnetic field. One of the hallmarks of graphene is the relativistic integer quantum Hall effect, manifested in a series of conductance plateaus at half-integer multiples of $4e^2/h$ [3,4,17]. Such unique QH plateau structure can be attributed to an odd number of QH edge states that carry current with conductance $2e^2/h$ [18,19]. The capability of placing local tunable electrostatic barriers or wells along the current pathway allows us to use QH mode propagation to explore intrinsic transport characteristics of graphene heterojunction structures.

Figure 3(a) shows $G(V_{\mathrm{LG}}, V_{\mathrm{BG}})$ at high magnetic field B for a typical device. In addition to the four regions seen at zero field [Fig. 3(a), inset], the conductance map reveals a rich pattern consisting of rhombi and bands where G exhibits plateaus. Overall this pattern is symmetric with respect to the neutrality point (marked with a black cross) which corresponds to $\nu = \nu' = 0$. (Here ν and ν' are the Landau level filling factors, equal to $n_c e/hB$ with n_c the carrier density in GLs and LGR, respectively.) While the plateaus in conductance at high densities $|\nu|, |\nu'| \geq 6$ are well accounted for by a two resistors-in-series model, with each resistor corresponding to the QH conductance of GLs, a more complex and interesting behavior is observed at lower densities, where resistors cease to add up in a classical fashion.

The nonclassical behavior is found at low filling factors, especially when either ν' or ν equals $+2$ or -2 [light gray traces near the top of Fig. 3(a) (red and orange online)]. Notably, we observe conductance plateaus at values close to fractional values of the conductance quantum, e^2/h. Such simple fractions include, for example, $(2/3)e^2/h$, $(6/7)e^2/h$, and $(10/9)e^2/h$ [Fig. 3(b)]. These values are in sharp contrast to the conductance plateaus at $(2, 6, 10, \ldots)e^2/h$, observed in homogenous two-terminal devices [7].

The unusual fractional conductance plateau patterns can be analyzed by using models developed for QH effect mode propagation in 2DEGs with density gradients [20,21]. Our graphene system, however, represents a distinct advantage owing to the possibility of creating opposite polarities of charge carriers in adjacent regions.

The simplest case to consider is when the polarity of GLs and LGR is the same (either n-n'-n or p-p'-p), and the LGR density is lower than the GLs' density: $|\nu'| \leq |\nu|$. In this case, as shown in Fig. 3(d), the number of QH edge modes is larger in the GLs than in the LGR. The modes

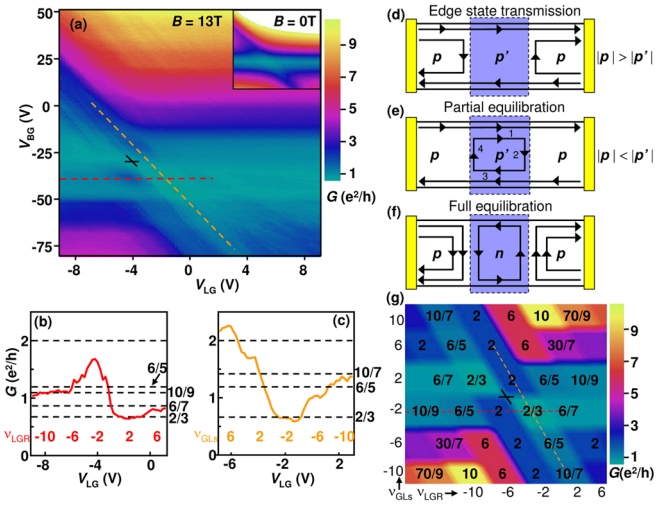

FIG. 3 (color online). (a) Color map of conductance $G(V_{\mathrm{LG}}, V_{\mathrm{BG}})$ at magnetic field $B = 13$ T, and $T = 4.2$ K. The black cross indicates the location of filling factor zero in LGR and GLs. Inset: Conductance at zero B in the same $(V_{\mathrm{LG}}, V_{\mathrm{BG}})$ range and the same color scale as main figure (white denotes $G > 10.5e^2/h$). (b) $G(V_{\mathrm{LG}})$ extracted from (a), solid line (red online), showing fractional values of the conductance. Numbers on the right indicate expected fractions for the various filling factors [numbers below the trace (red online) indicate the filling factor, ν', in LGR]; see also (g). (c) $G(V_{\mathrm{LG}})$ [projection of diagonal trace (orange online) from (a) onto V_{LG} axis]. Numbers below the trace (orange online) indicate filling factor, ν, in the GLs. (d), (e), and (f) different edge state diagrams representing possible equilibration processes taking place at different charge densities in the GLs and LGR. The center shaded (purple online) region indicates the LGR. Left and right light gray (yellow online) boxes indicate contact electrodes. (g) Simulated color map of the theoretical conductance plateaus expected from the mechanisms shown in (d), (e), and (f) for different filling factors in the GLs and LGR. The numbers in the rhombi indicate the conductance at that plateau. The color scale is identical to that of (a).

existing only in the GLs are fully reflected at the LGR-GLs interfaces [20,21], while those present in both regions exhibit full transmission, giving rise to the net conductance $G = (e^2/h)|\nu'|$.

A more interesting situation occurs when the LGR density is higher than the GLs' density, with the LGR and GLs' polarities still the same. In this case the number of edge states is smaller in the GLs than in the LGR [see Fig. 3(e)]. Crucially, the states circulating in LGR can produce partial equilibration among the different channels, because they couple modes with different electrochemical potentials. To analyze this regime, we suppose that current I is injected from the left lead, while no current is injected from the right lead. Then the conservation of current yields $I + I_4 = I_1$, $I_2 = I_3$ [the LGR edges are labeled by 1, 2, 3, 4 as shown on Fig. 3(e)]. Assuming that the current at the upper and lower LGR edges is partitioned equally among available edge modes, we obtain the relations for the current flowing out of these edges: $I_2 = rI_1$, $I_4 = rI_3$, $(r = 1 - \nu/\nu')$. Solving these equations for $I_{1\ldots4}$, we determine the current flowing in the drain lead as $I_{\mathrm{out}} = I_1 - I_2$ and find the net conductance

$$G = \frac{e^2}{h}\frac{|\nu'||\nu|}{2|\nu'| - |\nu|} = \frac{6}{5}, \frac{10}{9}, \frac{30}{7}, \ldots \quad (|\nu'| \geq |\nu|), \quad (1)$$

where $\nu = \nu' = \pm 2, \pm 6 \ldots$. We emphasize that this *partial equilibration* regime can only occur in the presence of two n-n' or p-p' interfaces, and would not occur in a single n-n' or p-p' junction [15,22].

The last, but most unique, case is when the GLs and LGR have opposite carrier polarity. In this case, the edge states counter-circulate in the p and n areas, running parallel to each other along the p-n interface [see Fig. 3(f)]. Such propagation, leading to mixing among edge states, results in full equilibration at the p-n interfaces: $I_1 = rI_2$, $I_3 = rI_4$, $(r = |\nu'|/(|\nu| + |\nu'|))$. Combining this with current conservation, in this case written as $I + I_1 = I_4$, $I_2 = I_3$, we find the currents and obtain the conductance

$$G = \frac{e^2}{h}\frac{|\nu'||\nu|}{2|\nu'| + |\nu|} = \frac{2}{3}, \frac{6}{5}, \frac{6}{7}, \ldots \quad (\nu\nu' < 0), \quad (2)$$

where ν, $\nu' = \pm 2, \pm 6 \ldots$. The net conductance in this case is described by three quantum resistors in series.

The summary of all possible conductance values for these three regimes is shown as a color map in Fig. 3(g). Our first observation is that the structure of the experimental pattern resembles qualitatively the theoretical one when the filling factor equals ± 2 either in the GLs or in the LGR. For a quantitative analysis, we choose two cuts extracted from Fig. 3(a), showing conductance for fixed $\nu = -2$ [Fig. 3(b)] and $\nu' = 2$ [Fig. 3(c)]. We record reasonably good plateaus at $G = (2/3)e^2/h$, $G = (10/9)e^2/h$ as well as other fractions discussed above, with the only exception of a considerably poorer plateau with $G = 2e^2/h$ (see below). Of particular interest is the nonmonotonic conductance behavior in Fig. 3(b) for $\nu' = 2, -2, -6, -10$ (with $\nu = -2$), which reflects the full equilibration → edge state transmission → partial equilibration sequence. This is in contrast to the monotonic behavior of G in Fig. 3(c) for $\nu = -2 \rightarrow 2 \rightarrow 6$ (with $\nu' = 2$), where only the full equilibration and full transmission regimes are expected.

We have measured in total four devices, which all exhibit similar conductance patterns. Notably, in none of these devices G reached the full $2e^2/h$ value at ν', $\nu = \pm 2$, whereas other conductance plateaus were well developed. The lack of quantization points to the presence of backscattering between opposite edges of our sample, which may occur in LGR bulk or in the transitional regions at the LGR-GLs junctions.

Why are the ν', $\nu = \pm 2$ plateaus so sensitive to backscattering, while other plateaus are not? To gain insight into this question, we now investigate how robust the

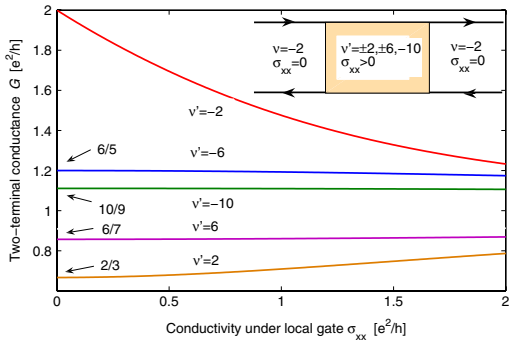

FIG. 4 (color online). Two-terminal conductance of a lateral heterojunction in a QH state (see inset) as a function of the longitudinal conductivity under local gate (LGR) for the states with $\nu = -2$ and $\nu' = \pm 2,\ \pm 6,\ -10$ [horizontal trace in Fig. 3(a) and solid line in Fig. 3(b), both red online]. Results obtained from the 2D transport model [23–25] for LGR of size 500 nm × 700 nm are shown. Finite σ_{xx} has considerable effect on the conductance of the state with ν', $\nu = -2$, but very little effect on other states. This explains the difference in roughness of the observed plateaus for $\nu' \neq -2$ and $\nu' = -2$.

results (1) and (2) are with respect to bulk conduction in our QH system. To that end, we consider a 2D transport model describing the system by local conductivity. Here we focus on the simplest situation, taking the longitudinal conductivity σ_{xx} nonzero in the gated region (LGR) and zero outside (GLs), and the Hall conductivity σ_{xy} equal to $\nu' e^2/h$ ($\nu e^2/h$) for LGR (GLs).

An exact solution for 2D current and potential distribution for this problem was obtained [23] by adapting the conformal mapping technique developed in Refs. [24,25]. The resulting two-terminal conductance G of the fractionally quantized states from the $\nu = -2$ trace [Fig. 3(b)] are displayed in Fig. 4. First, we note that the limiting values of G at $\sigma_{xx} \to 0$ agree with the simple fractions (1) and (2) derived above. Furthermore, the effect of finite σ_{xx} is considerably stronger for the $\nu = \nu' = -2$ state than for all other states—it is linear rather than quadratic at small σ_{xx}. Comparing it to the deviation from the quantized value in Fig. 3, we estimate $\sigma_{xx} \lesssim 0.5 e^2/h$.

We thus infer that weak backscattering is nondetrimental for all the states except $\nu = \nu'$, which is in agreement with the observed stability of fractional plateaus. This conclusion also agrees with the general intuition that current paths in a QH system are constrained more strongly when density is varying in space than when it is constant [26]. We therefore believe that our understanding of the stability of the observed fractional plateaus is quite generic and insensitive to whether the backscattering in our graphene devices occurs mainly in LGR bulk or at the LGR-GLs interfaces.

We thank A. Yacoby, C. Marcus, E. Poortere, and K. Bolotin for stimulating discussions, Inanc Meric for help with the ALD system, and Yang Wu for the Raman characterization. This work is supported by the ONR (No. N000150610138), FENA, NSF CAREER (No. DMR-0349232) and NSEC (No. CHE-0117752), and the New York State Office of Science, Technology, and Academic Research (NYSTAR). D. A. and L. L. acknowledge support by NSF MRSEC (No. DMR 02132802) and NSF-NIRT No. DMR-0304019.

Note added.—During the preparation of this manuscript, we became aware of related work on graphene p-n junctions [9,15,22].

*Corresponding authors.
†pk2015@columbia.edu

[1] K. S. Novoselov *et al.*, Science **306**, 666 (2004).
[2] A. K. Geim and K. S. Novoselov, Nat. Mater. **6**, 183 (2007).
[3] K. S. Novoselov *et al.*, Nature (London) **438**, 197 (2005).
[4] Y. Zhang, Y. W. Tan, H. L. Stormer, and P. Kim, Nature (London) **438**, 201 (2005).
[5] K. S. Novoselov *et al.*, Nature Phys. **2**, 177 (2006).
[6] Y. Zhang *et al.*, Phys. Rev. Lett. **96**, 136806 (2006).
[7] H. B. Heersche, P. Jarillo-Herrero, J. B. Oostinga, L. M. K. Vandersypen, and A. F. Morpurgo, Nature (London) **446**, 56 (2007).
[8] M. C. Lemme, T. J. Echtermeyer, M. Baus, and H. Kurz, IEEE Electron Device Lett. **28**, 282 (2007).
[9] B. Huard, J. A. Sulpizio, N. Stander, K. Todd, B. Yang, and D. Goldhaber-Gordon, Phys. Rev. Lett. **98**, 236803 (2007).
[10] V. V. Cheianov and V. I. Fal'ko, Phys. Rev. B **74**, 041403 (2006).
[11] V. V. Cheianov, V. Fal'ko, and B. L. Altshuler, Science **315**, 1252 (2007).
[12] A. Rycerz, J. Tworzydlo, and C. W. J. Beenakker, Nature Phys. **3**, 172 (2007).
[13] P. G. Silvestrov and K. B. Efetov, Phys. Rev. Lett. **98**, 016802 (2007).
[14] B. Trauzettel, D. V. Bulaev, D. Loss, and G. Burkard, Nature Phys. **3**, 192 (2007).
[15] J. R. Williams, L. C. DiCarlo, and C. M. Marcus, Science **317**, 638 (2007).
[16] A. C. Ferrari *et al.*, Phys. Rev. Lett. **97**, 187401 (2006).
[17] V. P. Gusynin and S. G. Sharapov, Phys. Rev. Lett. **95**, 146801 (2005).
[18] N. M. R. Peres, F. Guinea, and A. H. C. Neto, Phys. Rev. B **73**, 125411 (2006).
[19] D. A. Abanin, P. A. Lee, and L. S. Levitov, Phys. Rev. Lett. **96**, 176803 (2006).
[20] R. J. Haug, A. H. MacDonald, P. Streda, and K. von Klitzing, Phys. Rev. Lett. **61**, 2797 (1988).
[21] R. J. Haug, Semicond. Sci. Technol. **8**, 131 (1993).
[22] D. A. Abanin and L. S. Levitov, Science **317**, 641 (2007).
[23] D. A. Abanin and L. S. Levitov (unpublished).
[24] R. W. Rendell and S. M. Girvin, Phys. Rev. B **23**, 6610 (1981).
[25] R. Ilan, N. R. Cooper, and A. Stern, Phys. Rev. B **73**, 235333 (2006).
[26] W. Pan *et al.*, Phys. Rev. Lett. **95**, 066808 (2005).